Geophys. J. Int. (2001) **145,** 604–614

Magnetic properties and geochemistry of the active oxidation front and the youngest sapropel in the eastern Mediterranean Sea

H. F. Passier,[1] G. J. de Lange[2] and M. J. Dekkers[1]

[1] *Geodynamic Research Institute, Palaeomagnetic Laboratory 'Fort Hoofddijk', Budapestlaan* 17, 3584 CD *Utrecht, the Netherlands.*
E-mails: hpassier@geo.uu.nl, dekkers@geo.uu.nl
[2] *Institute of Palaeoenvironments and Palaeoclimate Utrecht, Geochemistry,* PO Box 80021, 3508 TA *Utrecht, the Netherlands*

Accepted 2000 November 30. Received 2000 November 30; in original form 2000 May 10

SUMMARY

Magnetic properties (IRM, ARM, χ_{in}, S-ratio at 0.3 T, room temperature (RT) hysteresis and thermomagnetic curves) and geochemical data (Fe, S, Mn, Al, Ti, organic C) were studied in two eastern Mediterranean boxcores (ABC26 and BC19) at a resolution of 3–5 mm. The boxcores contain sapropel S1 (9–6 kyr BP) at a few decimetres below seafloor. The magnetic fraction consists predominantly of single-domain (SD) to pseudo-single-domain (PSD) magnetite in the entire cores. The original input of magnetic grains comes from two sources: aeolian dust (both cores) and volcanic ash from the Minoan eruption of Santorini (core BC19 only). Non-steady-state diagenesis has changed the magnetic mineralogy considerably in these alternating organic-rich/organic-poor sediments. During deposition of sapropel S1, reductive diagenesis and pyritization in and just below the sapropel caused lower magnetic intensities, coarser magnetic grain sizes and partial maghemitization. In thermomagnetic curves two types of pyrite can be identified: one oxidizes below 450 °C and the other above 450 °C. The higher oxidation temperature is predominantly found below the sapropel. This may be related to the microtexture of pyrite, which is euhedral below sapropels and mainly framboidal within sapropels. Since the end of sapropel deposition a downward moving oxidation front has oxidized the upper half (*c*. 5 cm) of the sapropel. The oxidized part of the sapropel is enriched in diagenetically formed Fe oxides with relatively high coercivity and ARM. The maximum coercivity is found in a distinct layer between the present-day Mn- and Fe-redox boundaries at the top of the unoxidized sapropel. The freshly precipitated Fe oxides in this centimetre-thick layer contain a mixture of superparamagnetic (SP) grains and high-coercivity SD magnetite. Higher in the oxidized zone the freshly precipitated Fe oxides have aged into generally slightly lower-coercivity SD grains, with relatively high ARM. In addition to the diagenetic formation of Fe oxides at the top of the sapropel, formation of a ferrimagnetic Fe monosulphide may have occurred within the sapropel during later stages of diagenesis, which may have enhanced the ARM signal in the organic-rich interval in particular.

Key words: geochemistry, magnetite, marine sediments, Mediterranean Sea, oxidation, sediment magnetism.

1 INTRODUCTION

The most recent organic-rich sediment layer (sapropel) in the eastern Mediterranean Sea is situated a few decimetres below the sediment–water interface. It is called S1 (also Si2 after Lourens *et al*. 1996) and was deposited between 9 and 6 kyr BP (Rossignol-Strick 1999). More than 80 sapropels occur in Pliocene to Holocene eastern Mediterranean sediments (e.g. Emeis & Party 1996). Sapropel formation is related to enhanced productivity and increased preservation of organic matter during periods with a relatively wet climate. These climate conditions are related to precession-induced insolation maxima (Rossignol-Strick *et al*. 1982; Calvert *et al*. 1992; Rohling 1994). They invoke enhanced run-off from rivers and changes in the circulation pattern within the eastern Mediterranean Sea. Aeolian dust input was reduced during sapropel deposition (Wehausen & Brumsack 1999).

Sapropels are a few centimetres to decimetres thick. Apart from being enriched in organic carbon, they contain pyrite as a result of bacterial sulphate reduction, which prevailed during

their deposition. This sulphate reduction also supplied sulphide that diffused to the sediments below the sapropel. Consequently, pyrite is also enriched in the interval directly below the sapropel. This interval can be up to several decimetres thick and is called 'synsapropel' in diagenetic context (Passier *et al.* 1996, 1997, 1999). Mediterranean bottom waters were reoxygenated at the end of the formation of sapropel S1 and oxic sediments have buried S1. An oxidation front is now situated at the top of the organic-rich layer. At this front, organic carbon and pyrite are oxidized by oxidants that diffuse downward from the bottom water to the front. As a result of this oxidation, the organic-rich layer has become progressively thinner and metal oxides have precipitated directly above it (e.g. de Pruysers *et al.* 1993; van Santvoort *et al.* 1996).

Magnetic Fe minerals are involved in many of the redox processes that occur in alternating organic-poor/organic-rich sediments. Therefore, diagenesis in sediment successions such as those found in the eastern Mediterranean, may significantly alter the sedimentary magnetic record. In suboxic and anoxic (sulphate-reducing) environments, magnetic Fe oxides dissolve, resulting in a decrease of magnetic intensities (Karlin & Levi 1985; Canfield & Berner 1987; Channell *et al.* 1990; Karlin 1990a,b; Leslie *et al.* 1990a,b; Robinson 1990; Bloemendal *et al.* 1993; Schwartz *et al.* 1997). On the other hand, precipitation of Fe oxides at an oxidation front causes higher magnetic intensities (Dekkers *et al.* 1994; Langereis *et al.* 1997; van Santvoort *et al.* 1997; Passier *et al.* 1998). Iron oxides around palaeo-oxidation fronts have been reported to have specifically high magnetic coercivity (Sahota *et al.* 1995; Tarduno & Wilkison 1996; Tarduno *et al.* 1998), that could indicate the presence of bacterial magnetite. Fe oxides are not the only magnetic Fe minerals that may be important in relation to sapropels; Roberts *et al.* (1999) reported the formation of magnetic Fe sulphides, especially in extremely organic-rich sapropels.

Here, we relate magnetic and geochemical data from two boxcores containing sapropel S1, sampled at subcentimetre resolution. Thus we can separate the effects of diagenesis and detrital input on sedimentary magnetic properties. We provide insight into the pathways of Fe-oxide formation at the active oxidation front, variations in aeolian dust input and the reductive diagenesis in and below S1. We demonstrate that within the relatively short geological period of <10 kyr, the magnetic mineralogy of these sediments undergoes significant alteration.

2 MATERIALS AND METHODS

2.1 Samples

Boxcore ABC26 (30 cm long) was recovered 200 km south of Crete (33°21.3′N, 24°55.7′E, water depth 2150 m) during the 1987 ABC expedition of R/V Tyro. Boxcore BC19 (35 cm long) was recovered in the Herodotus Abyssal Plain (33°47.8′N, 28°36.4′E, water depth 2750 m) during the 1991 MD69-Marflux expedition with R/V Marion Dufresne. Both boxcores contain sapropel S1, preceded by grey oozes and followed by cream to brown *pteropod*-rich ooze. Furthermore, the ash layer of the Minoan Eruption of Santorini (3.6 kyr BP) is present in BC19.

Subcores were sealed air-tight and stored vertically at 4 °C for 3 (ABC26) to 7 (BC19) yr before they were subsampled at resolutions of 3 and 5 mm for ABC26 and BC19, respectively. The sediment was dried (ABC26 in a stove at 60 °C, BC19 freeze-dried) and pulverized in an agate mortar. Tests with samples from a magnetically diverse zone in BC19 (at sediment depths of 217.5 and 232.5 mm) that were freeze-dried as well as dried in the stove at 60 °C proved that the different drying techniques did not influence the magnetic properties.

2.2 Geochemical analyses

A mixture of $HClO_4$ and HNO_3, and HF was added sequentially to dissolve the sediments (250 mg). After heating in closed Teflon containers (90 °C, 12 hr), the solution (10 mL) was evaporated on a sandbath-heater (180 °C). The dried residue was dissolved in 50 mL 1 M HCl for elemental analysis with an inductively coupled plasma atomic emission spectrometer [ARL 34000 (ABC26) or Perkin Elmer OPTIMA 3000 (BC19)]. Iron in pyrite (Fe_{pyr}) was calculated from the total S content assuming Fe:S = 1:2 in pyrite, and corrected for the non-pyritic base level amount of S. This calculation proved to be accurate to estimate the pyritic Fe content in S1, where the base level S is mainly pore-water sulphate and no other S phases are significant (Passier *et al.* 1999). Iron in Fe oxides (Fe_{ox}) was calculated from total Fe minus Fe_{pyr}, corrected for an estimated background value of Fe depending on Al (Fe/Al = 0.44 wt per cent/wt per cent), that is presumably residing in aluminosilicates. After removal of carbonate in 1 M HCl, organic carbon (C_{org}) contents were determined with a Fisons Instruments NA-1500 NCS analyser. Measurements on in-house and international standards indicate that all geochemical analyses have standard deviations of <5 per cent.

2.3 Magnetic measurements

Thermomagnetic runs in air from room temperature to 700 °C were carried out (ABC26 all samples, BC19 selected samples) with a modified horizontal translation-type Curie balance (sensitivity of *c.* 5×10^{-9} A m^2) (Mullender *et al.* 1993). Sediment (20–30 mg) was weighed into a quartz glass sample holder open to air and held in place by quartz wool. Heating and cooling rates were 10 °C min^{-1}.

Sediment (100 mg) was weighed into cylindrical vials (8 cm^3) and moulded in epoxy resin (Ciba araldite D, hardener HY 956). Initial susceptibility (χ_{in}) was measured at room temperature with a KLY-2 AGICO susceptometer (frequency 920 Hz; rms field strength 0.37 mT; noise level 4×10^{-8} SI). Measurements were corrected for the blank signal of epoxy resin in vials without sediment. Anhysteretic remanent magnetization (ARM) was induced with peak alternating fields (AFs) of 75, 100, 125, 150, 200 and 300 mT in a direct current bias field of 29 μT parallel to the AF. Next, the ARM acquired at 300 mT ($ARM_{300\ mT}$) was stepwise demagnetized in alternating fields of 5, 10, 20, 30, 40, 50, 75, 100, 150, 200 and 300 mT in three orthogonal directions. Saturation isothermal remanent magnetization (M_{rs}) was induced with a PM4 pulse magnetizer in a field of 2 T. Then, the M_{rs} was stepwise demagnetized at the same steps as the ARM. For calculation of the S-ratio [$1-(IRM_{-0.3\ T}/IRM_{1\ T})/2$; Bloemendal *et al.* 1992], IRM was induced in a field of 1 T and subsequently in a backfield of 0.3 T. ARM and IRM intensities were measured with a JR5A AGICO spinner magnetometer (noise level 3×10^{-11} A m^2), a 2G Enterprises DC SQUID magnetometer (noise level 4×10^{-12} A m^2), or a 2G Enterprises RF SQUID magnetometer (noise level 1×10^{-11} A m^2).

To measure hysteresis loops at room temperature (B = +1 T to −1 T), 100–200 mg sediment was weighed into a gelatine capsule and placed in a plastic drinking straw. Hysteresis measurements were made with a Princeton Measurements Corporation vibrating sample magnetometer (Micro VSM, sensitivity 2×10^{-8} A m^2) at the Institute for Rock Magnetism (IRM, Minneapolis, USA). The coercive force (B_c), the remanent saturation magnetization (M_{rs}) and the saturation magnetization (M_s) were determined from the loops.

3 RESULTS

3.1 Geochemistry

The geochemical data allow identification of different zones in the sediments. C_{org} (Fig. 1) is enriched in S1 (up to 2.6 wt per cent in ABC26 and up to 3.9 wt per cent in BC19), while non-sapropel sediments have C_{org} contents of 0.1–0.4 wt per cent. The highest contents of Fe_{pyr} (Fig. 1) are found within the sapropel (up to almost 3.5 wt per cent). Fe_{pyr} is also enriched in the interval directly below S1.

Fe_{ox} (Fig. 1) is enriched above the sapropel, and maximum contents (1.9 wt per cent in ABC26 and 3.1 wt per cent in BC19) are found at the top of the sapropels. Manganese is enriched up to 1 wt per cent above the sapropels (Fig. 1). There are two Mn maxima, which both consist of Mn oxides (van Santvoort *et al.* 1996). The uppermost maximum, situated at depths of 135 mm in ABC26 and 168 mm in BC19, marks the original thickness of the sapropel before it was oxidized (van Santvoort *et al.* 1996). The other Mn peak is situated immediately above the organic-rich layer (van Santvoort *et al.* 1996). Above this peak, Mn oxides are stable, below the peak dissolved Mn(II) is present (van Santvoort *et al.* 1996). This sedimentary level is the Mn–redox boundary (MnRB). In a small zone below the MnRB, Fe oxides may be formed via the oxidation of Fe by Mn oxides and/or nitrate. The Mn contents decrease from the maximum to background values (Fig. 1) in this zone. The lower border of this zone is the Fe–redox boundary (FeRB). Below the FeRB dissolved Fe(II) is present, while above the boundary solid Fe oxides are stable.

Ti/Al varies between 0.06 and 0.07 wt per cent/wt per cent in both cores (Fig. 2), with a minimum of 0.04 wt per cent/wt per cent present in the ash layer. Correction for dilution by carbonate assuming a constant Al flux does not change the geochemical profiles.

3.2 Thermomagnetic analyses

Curie points are around 600 °C in the uppermost 23 cm of BC19 and 20 cm of ABC26 (latter not shown), including the oxidized part of the sapropel, which indicates the predominance of magnetite (Fig. 3). The presence of titanomagnetite and maghemite cannot be excluded. Apart from the crystalline magnetic Fe oxides, amorphous Fe oxide is an important constituent of the sediments. This is deduced from the initial magnetization in thermomagnetic analyses, which averages 0.02 A m^2 kg^{-1}. This magnetization would be two orders of magnitude higher if all Fe oxides (Fe_{ox}; Fig. 1) were crystalline magnetite or maghemite with saturation magnetization of about 90 A m^2 kg^{-1}.

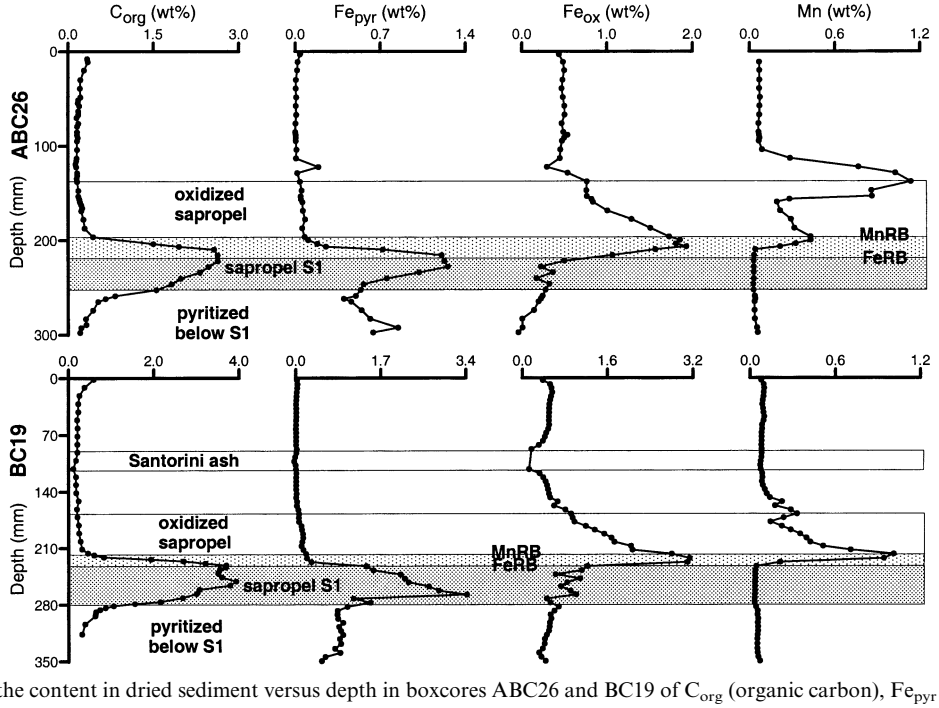

Figure 1. Profiles of the content in dried sediment versus depth in boxcores ABC26 and BC19 of C_{org} (organic carbon), Fe_{pyr} (pyritic Fe, calculated from total S contents, assuming a ratio of 1:2 of Fe:S in pyrite, after correction for a constant background S content), Fe_{ox} (Fe in Fe oxides, i.e. total Fe minus Fe_{pyr}, corrected for background Fe contents that depend on Al contents) and Mn (total Mn). Fe_{ox} was not calculated in the ash layer in BC19 because background Fe cannot be estimated here. The shaded band is the unoxidized part of sapropel S1; the light part of this band is the zone between the Mn and Fe redox boundaries (MnRB and FeRB), where active Fe oxide precipitation takes place. Different sediment zones have been indicated: oxidized sapropel, sapropel, pyritized zone below S1 and Santorini ash layer.

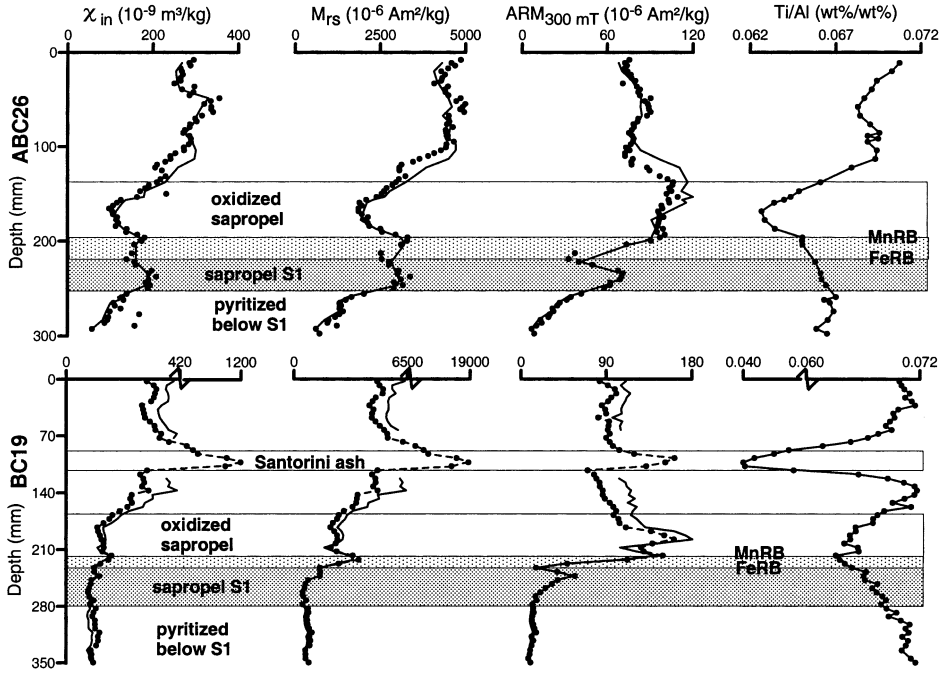

Figure 2. Profiles of χ_{in}, M_{rs}, $ARM_{300\ mT}$, and Ti/Al versus depth in boxcores ABC26 and BC19. Points and dashed lines represent uncorrected data, solid lines (except Ti/Al) represent carbonate-corrected data assuming a constant Al flux (that is, division of a value by the Al content of a specific sample and multiplication by the average Al content). The ash layer was not included in the carbonate correction because the Al flux presumably varied significantly in this layer. See Fig. 1 for explanation of different sediment zones.

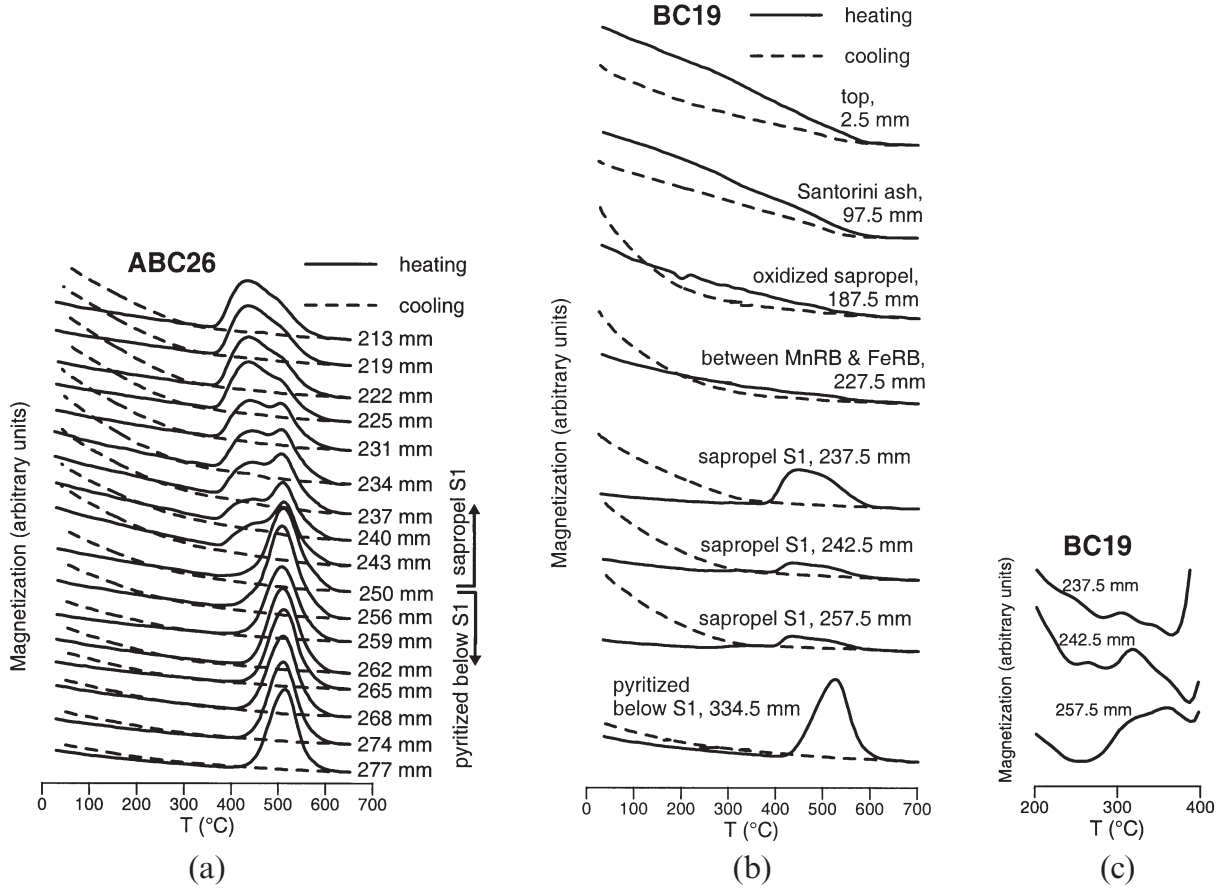

Figure 3. Selected thermomagnetic curves measured on a Curie balance in air from different sediment zones in boxcores: **(a)** ABC26, (b) BC19 and **(c)** enlargement of part of the heating curves in the sapropel in BC19.

After heating to 700 °C, the magnetic Fe oxides are largely destroyed and the cooling curves generally show lower magnetizations than the heating curves. In contrast, cooling curves in the oxidized part of the sapropel undergo rapidly increasing magnetizations towards room temperature. There is a increase in magnetization, proportional to $1/T$, during cooling, which indicates that (super)paramagnetism is responsible for the observed increase in magnetization. Possibly, fine-grained, superparamagnetic Fe oxides formed at higher temperatures.

In the sapropel and directly below it, pyrite can be identified in the thermomagnetic curves through its oxidation to magnetite and maghemite and finally to haematite, which causes an increase and subsequent decrease in magnetization (Fig. 3). The humps in the thermomagnetic curves often consist of two peaks, indicating a phase that oxidizes below 450 °C and another that oxidizes above 450 °C. In the pyritized zone below the sapropel, only the higher oxidation temperature is found. A small increase in magnetization between 250 and 400 °C is observed in some sapropel samples from BC19 (Fig. 3c) but not in ABC26 (Fig. 3a).

3.3 Remanences and susceptibility

χ_{in}, M_{rs}, and $ARM_{300\ mT}$ vary according to the content of magnetic minerals. These parameters may also depend on grain size and mineralogy (e.g. Banerjee *et al.* 1981; King *et al.* 1982; Maher 1988; Heider *et al.* 1992).

M_{rs} values vary between 500×10^{-6} and 5000×10^{-6} A m^2 kg^{-1} and χ_{in} between 50×10^{-9} and 360×10^{-9} m^3 kg^{-1}, with the exception of the ash layer with χ_{in} of almost 1200×10^{-9} m^3 kg^{-1}, and M_{rs} of about 19×10^{-3} A m^2 kg^{-1} (Fig. 2). The highest values are found in the top of the cores and the lowest values are found below sapropel S1. If χ_{in} is below 10^{-4} SI (Frederichs *et al.* 1999), which corresponds to $\sim 35 \times 10^{-9}$ m^3 kg^{-1}, the diamagnetic contribution of biogenic carbonate should be taken into account. The sediments investigated here have higher $\chi_{in,}$ so diamagnetism may be neglected. Correction for carbonate dilution does not significantly change the profiles of the magnetic parameters (Fig. 2). The patterns of χ_{in} with depth are similar to those of M_{rs} ($R^2 = 0.91$ for both ABC26 and BC19), which suggests that variations in χ_{in} is governed by the same ferrimagnetic minerals as M_{rs} and not significantly influenced by paramagnetic minerals like clays. The variations in M_{rs} and χ_{in} generally correlate well with the Ti/Al pattern (Fig. 2). Exceptions are the ash layer where Ti/Al is extremely low and the lower parts of the cores where M_{rs} and χ_{in} are low relative to Ti/Al. Outside these exceptional areas correlation (R^2) between Ti/Al and χ_{in} are 0.81 and 0.70 for ABC26 and BC19, respectively; between Ti/Al and M_{rs} they are 0.84 and 0.54, respectively.

$ARM_{300\ mT}$ values range between 70×10^{-6} and 100×10^{-6} A m^2 kg^{-1} in the upper part of the boxcores (Fig. 2). A peak is present (160×10^{-6} A m^2 kg^{-1}) in the ash layer. $ARM_{300\ mT}$ is high within the oxidized part of the sapropel, up to 160×10^{-6} A m^2 kg^{-1} in BC19 and up to 110×10^{-6} A m^2 kg^{-1} in ABC26. A local minimum is present in the upper part of the remaining sapropel. Low values of $ARM_{300\ mT}$ of $5 \times 10^{-6} - 10 \times 10^{-6}$ A m^2 kg^{-1} are found in the pyritized zone below S1. Correction for carbonate dilution does not significantly change the profiles of $ARM_{300\ mT}$ (Fig. 2).

3.4 Grain size and coercivity

The median destructive fields of ARM (MDF_{ARM}) and IRM (MDF_{IRM}) and B_c are highly variable with depth (10–100 mT) and have similar patterns (Fig. 4). These parameters are relatively low in the upper sediments, they are higher in the oxidized sapropel. They are extremely high between the MnRB and the FeRB and intermediate in the lower part of the sapropel and in the pyritized zone below S1.

The S-ratio indicates the relative importance of low-coercivity versus high-coercivity grains. The S-ratio is relatively high in the upper part of BC19 and ABC26, with maxima (0.98) in the ash layer and in the oxidized sapropels. It is lower in the sapropel and the pyritized zone below S1, with a minimum in the top of the sapropels between the MnRB and FeRB (0.81 in ABC26 and 0.66 in BC19; Fig. 4). The minimum S-ratio is slightly deeper in the sediment than the maxima of MDF_{ARM}, MDF_{IRM} and B_c.

The ratio between χ_{ARM} ($ARM_{300\ mT}$ intensity divided by the bias field) and χ_{in} depends on the grain-size distribution of magnetite, if magnetite is the dominant magnetic mineral. χ_{ARM}/χ_{in} decreases from SD via PSD to MD grains. SP grains also have low χ_{ARM}/χ_{in} (King *et al.* 1982; Bloemendal *et al.* 1992). χ_{ARM}/χ_{in} values (Fig. 5) are all in the SD–PSD size range. The ratio varies from 5 to 7 in the tops of the cores. The ash layer has a minimum ratio of 2.8. χ_{ARM}/χ_{in} is higher than 20 in the oxidized sapropel, further down it decreases, with

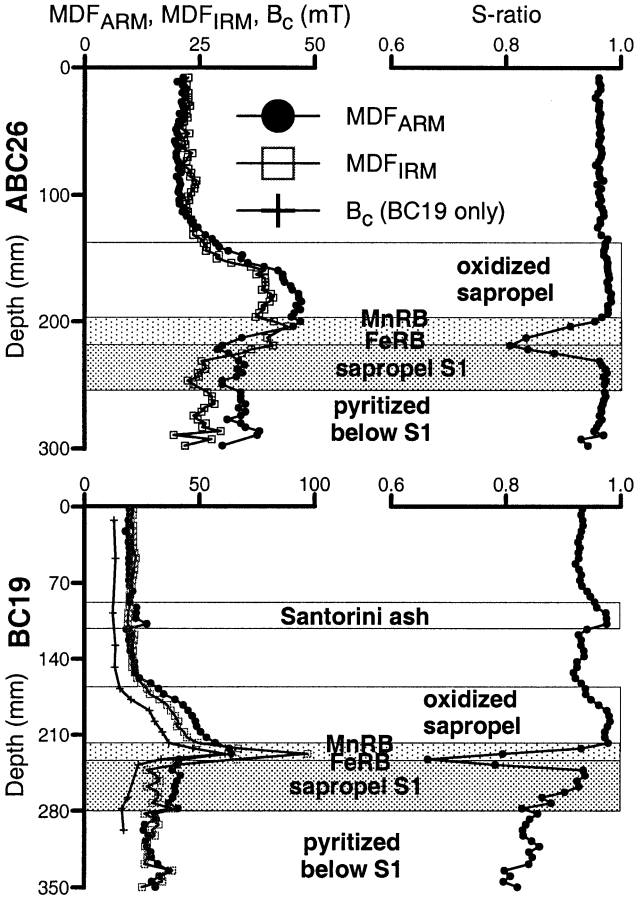

Figure 4. Profiles of MDF_{ARM}, MDF_{IRM}, B_c, and S-ratio $[=1-(IRM_{-0.3T}/IRM_{1T})/2]$ versus depth in boxcores ABC26 and BC19. See Fig. 1 for explanation of different sediment zones.

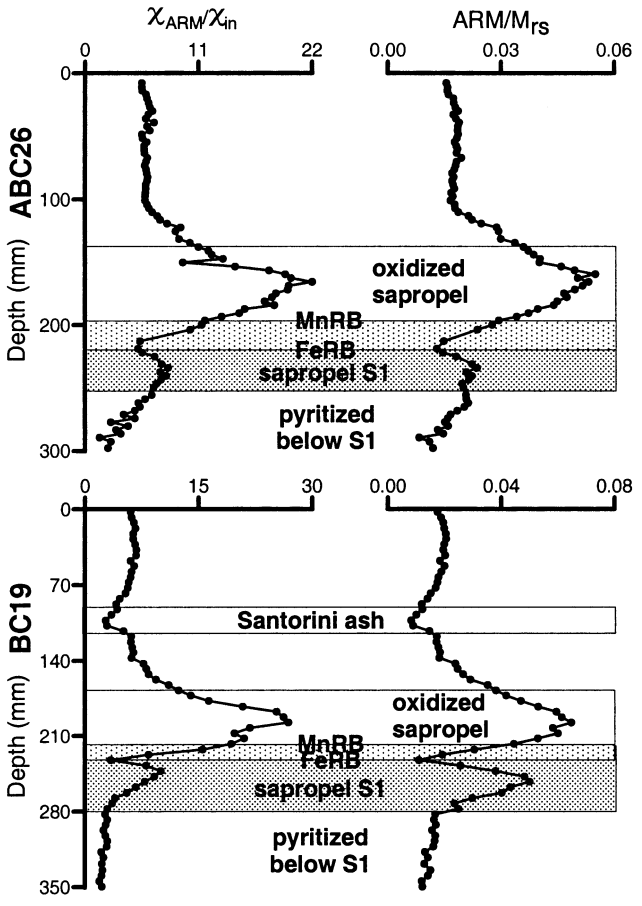

Figure 5. Profiles of χ_{ARM}/χ_{in} and ARM/M_{rs} versus depth in boxcores ABC26 and BC19. See Fig. 1 for explanation of different sediment zones.

a local minimum (3–5) in the top of the sapropel. χ_{ARM}/χ_{in} is lowest below the sapropels. ARM/M_{rs} is also a grain-size indicator, with lower values for coarser grain sizes. The ARM/M_{rs} profiles (Fig. 5) are similar to the χ_{ARM}/χ_{in} profiles.

3.5 Hysteresis loops

The hysteresis loops of samples from BC19 (Fig. 6) have been corrected for a paramagnetic high-field slope. All loops suggest that samples achieved saturation. The loops have parallel up- and down-going branches in the top of the core, indicating grain sizes that are coarser than SD. The loops at 187.5, 197.5 and 207.5 mm in the oxidized part of the sapropel have a wide centre and slouching shoulders, i.e. a pot-belly shape. This shape is typical of SD grains, or mixtures of SD and SP grains (Tauxe *et al.* 1996). The loops at 222.5, 227.5, 232.5 and 237.5 mm clearly have constricted middles, i.e. wasp-waists. Wasp-waisted hysteresis loops like these have been reported for mixtures of low- and high-coercivity minerals and for mixtures of two grain-size fractions of the same mineral, such as SD and large SP grains (Roberts *et al.* 1995; Tauxe *et al.* 1996). M_{rs}/M_s in BC19 (Fig. 6) is between 0.2 and 0.5, i.e. in the PSD size range (Thompson & Oldfield 1986), with higher values in the oxidized sapropel, and a maximum in the top of the sapropel.

4 DISCUSSION

The measured magnetic parameters reflect not only variations in the input of detrital minerals, but also the diagenetic processes that occurred in these eastern Mediterranean sediments since their deposition. First, we will discuss clear detrital signals and then we will consider differences between several diagenetic zones in the boxcores.

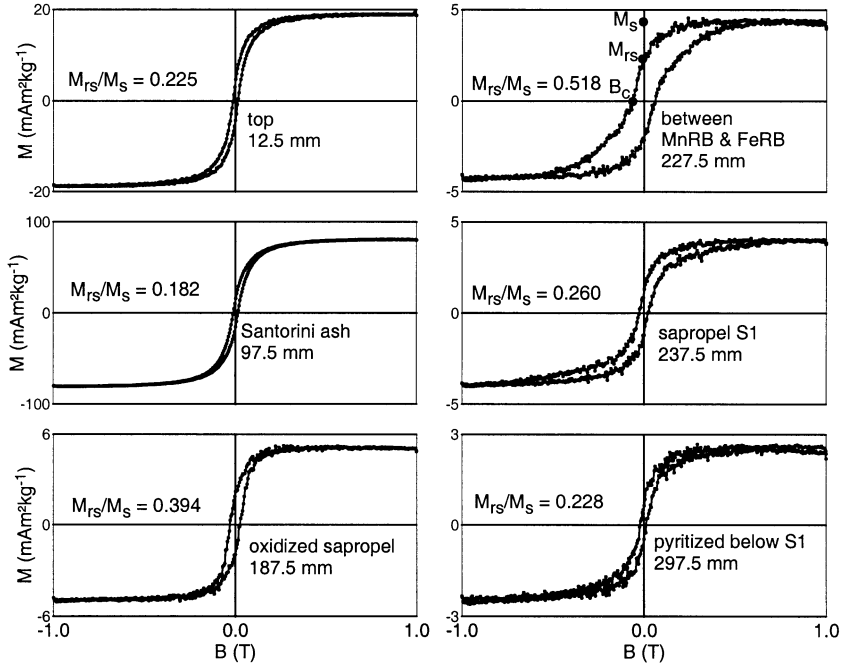

Figure 6. Selected hysteresis loops and M_{rs}/M_s values from different sediment zones in boxcore BC19.

4.1 Detrital signals

4.1.1 Aeolian input

Ti/Al values of eastern Mediterranean sediments correlate with aeolian dust contents. The aeolian input was lower during the humid climate of sapropel formation, whereas river input was higher, resulting in lower Ti/Al values around and within sapropels (Wehausen & Brumsack 1999). The Ti/Al variations above the sapropels, apart from the ash layer, correlate with M_{rs} and χ_{in} (Fig. 2). The correlation between Ti/Al and M_{rs} and χ_{in} suggests that dust was the main source of ferrimagnetic grains in the sediment before it was affected by suboxic/anoxic diagenesis. Magnetic measurements of the surface sediments indicate that the original magnetic grains are SD to PSD magnetite. The correlation between M_{rs} and χ_{in} is absent, however, in the lower parts of the cores, where M_{rs} and χ_{in} are low relative to Ti/Al. This may be caused by reductive dissolution of the magnetic grains carrying M_{rs} and χ_{in} (see Section 4.2). The $ARM_{300\ mT}$ signal has been affected more thoroughly by diagenesis than M_{rs} and χ_{in} (see Section 4.3); any possible pre-existing correlation of $ARM_{300\ mT}$ with Ti/Al has been erased.

4.1.2 Santorini ash layer

The ash layer deposited after the Minoan eruption of Santorini at 3.6 kyr BP is present in BC19, but not in ABC26. This is a result of the prevailing westerly wind direction. The layer is strongly magnetic. The magnetic measurements indicate that the magnetization is carried by PSD magnetite of a slightly larger grain size than found in the surrounding sediments.

4.2 Suboxic/anoxic diagenesis

4.2.1 Surface sediments versus pyritized zone below S1

Most probably, at the time of deposition, the sediments of the pyritized zone below S1 resembled the surface sediments, where Fe minerals are unaffected by suboxic/anoxic diagenesis. Anoxic conditions and subsequent pyrite formation at times of sapropel deposition caused reductive dissolution of Fe oxides in the pyritized zone below S1 (Passier *et al.* 1999). Reductive dissolution continues under the present suboxic conditions. Reductive dissolution is expressed in the relatively low intensities of $ARM_{300\ mT}$, M_{rs}, χ_{in} and M_s in the pyritized zone below S1 (Figs 2,4,6). The presence of pyrite in the pyritized zone below S1 is evident from the thermomagnetic analyses (Fig. 3).

Coercivities are higher in the pyritized zone below S1 than in the surface sediments and the S-ratio is lower (Fig. 4). These features may be caused by the partial maghemitization of magnetite during reductive dissolution. This partial maghemitization is possibly the result of the preferential diffusion of Fe(II) out of magnetite grains, as Fe(II) is more easily detached from the mineral structure than Fe(III) (Cornell & Schwertmann 1996). The magnetic grain size is relatively coarse (PSD) in the pyritized zone below S1, as suggested by the low χ_{ARM}/χ_{in} and ARM/M_{rs} ratios (Fig. 5). This may result from preferential dissolution of the finest-grained magnetic material during reductive dissolution (e.g. Leslie *et al.* 1990a).

4.2.2 Sapropel versus pyritized zone below S1

The sapropel and pyritized zone below S1 are enriched in pyrite that formed under anoxic sulphidic conditions during sapropel formation. Since sapropel formation, conditions have been suboxic in this zone of the sediment (Passier *et al.* 1999). The thermomagnetic curves in the sapropel and the pyritized zone below S1 are distinctly different. They reveal two types of pyrite, one oxidising below 450 °C and the other above 450 °C. In samples from the pyritized zone below S1, only the higher oxidation temperature is found. This correlates with the microtextures of pyrite: euhedral pyrite (crystals of 2–10 μm and aggregates) occurs in the pyritized zone below S1 and mainly framboidal pyrite (diameters of 5–10 μm, consisting of (sub)micron-sized microcrystals) occurs within sapropel S1 (Passier *et al.* 1997). Framboidal pyrite formed rapidly at high concentrations of sulphide and Fe at the site of bacterial sulphate reduction (i.e. sapropel S1). In contrast, diffusive fluxes of sulphide and Fe resulted in the relatively slow formation of euhedral pyrite in the pyritized zone below S1 (Passier *et al.* 1997) The reactive surface area in the framboids is larger than that of the euhedral pyrite. This could explain the lower oxidation temperature for pyrite in the sapropel.

The sediments in the unoxidized part of the sapropel (below the FeRB) show some of the features of reductive dissolution of magnetite such as those seen in the pyritized zone below S1, including slightly elevated coercivity parameters MDF_{ARM}, MDF_{IRM} and $B_{c,}$ compared to the uppermost sediments, and relatively low M_{rs}, $ARM_{300\ mT}$, χ_{in}, and M_s values (Figs 2, 4 and 6). However, the S-ratio and the intensity of magnetizations, especially $ARM_{300\ mT}$, are generally higher in the unoxidized sapropel than in the pyritized zone below S1. The high $ARM_{300\ mT}$ leads to high ratios of χ_{ARM}/χ_{in} and ARM/M_{rs} in the lower part of the sapropels (Fig. 5). These high values argue against reductive dissolution, which is remarkable, because reductive dissolution and pyrite formation have been at least as extensive in the sapropel as in the pyritized zone below S1 (Passier *et al.* 1999).

Possibly, the high χ_{ARM}/χ_{in} and ARM/M_{rs} in the lower part of the sapropels, relative to the pyritized zone below S1, are caused by the presence of a magnetic Fe sulphide phase as discussed by Roberts *et al.* (1999). These authors also found extremely high values for these ratios in the lower part of Mediterranean sapropels older than S1. Furthermore, the presence of a magnetic Fe sulphide phase in these older sapropels caused higher magnetic intensities and high S-ratios. The magnetic enhancement by magnetic Fe sulphides, however, seems related to the organic carbon content of the sapropels. The sapropels investigated by Roberts *et al.* (1999) contained at least twice as much organic carbon as S1. This could explain the absence of an extreme magnetic enhancement in S1. The magnetic Fe sulphide phase found by Roberts *et al.* (1999) exhibits an irreversible breakdown at 360 to 400 °C during heating in air. They described this phase as an unidentified ferrimagnetic Fe sulphide mineral having properties only broadly consistent with those of greigite. In the thermomagnetic analyses of some of the sapropel samples we identify a phase that breaks down between 250 and 400 °C to presumably form magnetite and/or maghemite, which causes an increase in magnetization (Fig. 3c). Unfortunately, the abundance of this phase is too low in S1 to be able to obtain more specific information about it.

Ferrimagnetic Fe monosulphides that form as precursors of pyrite could have formed during sapropel formation under pervasive sulphate reducing conditions (Passier *et al.* 1999) at the same time that the bulk of the pyrite formed. On the other hand, the Fe monosulphides may have been produced during later stages of diagenesis. The stable sulphur isotopic composition of Fe monosulphides found in an extremely organic-rich Pliocene sapropel (Passier *et al.* 1999) suggests that these Fe monosulphides were formed during more recent stages of diagenesis than the pyrite, because these monosulphides have a heavier sulphur isotopic composition than the pyrite. The formation of these Fe monosulphides during later stages of diagenesis could cause a palaeomagnetic overprint in these sapropel sediments. This may explain partly why magneto-stratigraphic results from Mediterranean cores are ambiguous despite the fact that the sediments record stable magnetizations (e.g. Richter *et al.* 1998).

4.3 Oxic diagenesis

4.3.1 The oxidized sapropel: review of diagenetic history

Since bottom waters were reoxygenated at the end of sapropel formation in the eastern Mediterranean, oxidants have diffused from the bottom waters into the sediments and oxidized the sapropel. The present site of active oxidation is at the top of the organic-rich layer (van Santvoort *et al.* 1996). Organic carbon and pyrite are oxidized at this oxidation front. The decrease of C_{org} starts at shallower depth in the cores than the decrease of Fe_{pyr} (Fig. 1). This indicates that the depth of oxidation of organic matter is shallower than the oxidation of pyrite. Apart from the presence of Fe^{3+}, oxidising bacteria, organic complexes of ferric iron and surface interactions with clay minerals may be important for the oxidation of pyrite and their exact roles in marine sediments are still unknown (Bierens de Haan 1991; Brothers *et al.* 1996). At the site of active oxidation of pyrite, sulphate and Fe^{2+} are liberated. The liberated Fe subsequently forms Fe oxides. Additionally, in the suboxic sediments below the oxidation front, Fe^{2+} is liberated in reductive dissolution of Fe oxides by bacteria. This liberated Fe^{2+} diffuses upwards to the front, where it precipitates as Fe oxides. The oxidation front has moved down into the sediment since the end of sapropel formation, forming Mn and Fe oxide enrichments in the place of the former sapropel (Fig. 1). The rate of downward movement of the front decreases with time, as the diffusion distance for oxidants increases. Eventually, the front comes to a standstill, when uptake of oxidants is in equilibrium with their downward diffusion.

The zone where Fe oxides are currently being formed is confined to the small zone between the MnRB and the FeRB. This zone of the sediment is characterized by oxidation of Fe^{2+} to a solid Fe oxide phase by Mn oxides and/or nitrate; bacteria may play an important role in this process (Burdige 1993; Tarduno *et al.* 1998). In this zone of the sediment, where there is a steep redox gradient from oxic to suboxic, magnetotactic bacteria may produce magnetosomes consisting of elongated SD magnetite in the narrow size range of $\sim$35–120 nm (Frankel & Bazylinski 1994; Bazylinski 1996). In addition, precipitated amorphous Fe oxide may chemically transform into more crystalline phases, and phases such as so-called 'green rust' [mixed Fe(II)-Fe(III) hydroxy salts], goethite, maghemite or magnetite may form under sedimentary pH and temperature conditions (Cornell & Schwertmann 1996).

4.3.2 The oxidized sapropel: magnetic properties

The Fe-oxide-rich oxidized sapropel (Fig. 1) is characterized by distinct magnetic properties. As a result of bioturbation, the distinct features extend a few centimetres above the oxidized sapropel.

$ARM_{300\ mT}$ values are relatively high in the oxidized sapropel, while M_{rs} and χ_{in} are not (Figs 2 and 4). Apparently, the newly formed Fe oxides are more prone to carry an $ARM_{300\ mT}$ than an IRM and their susceptibility is comparatively low. This indicates that specifically SD and small PSD magnetite grains are present in the oxidized sapropel. The high values of χ_{ARM}/χ_{in} and ARM/M_{rs} (Fig. 5) illustrate the dominance of $ARM_{300\ mT}$ in the oxidized sapropel, with χ_{ARM}/χ_{in} values that are indicative of small SD grains according to the diagram of Bloemendal *et al.* (1992). Thermomagnetic curves show the presence of magnetite and formation of ultrafine SP grains upon heating in air; the latter indicates that the diagenetic Fe oxides are relatively reactive.

Both coercivity and the Fe_{ox} values increase with depth in the oxidized sapropel (Figs 1 and 4). This correlation suggests that the increase in coercivity through the oxidation front can be partially explained by the addition of high-coercivity Fe oxides to the sediments. Between the MnRB and the FeRB, however, the increase in Fe oxides cannot account for the large increase in coercivity. The S-ratio is distinctly different in this zone. Extremely low S-ratios (due to relatively high contributions of high-coercivity minerals) are found between the MnRB and the FeRB (Fig. 4). Furthermore, the hysteresis loops (Fig. 6) measured at this level in BC19 are wasp-waisted, which indicates a mixture of relatively high- and low-coercivity grains that both contribute comparable amounts of magnetization (Roberts *et al.* 1995; Tauxe *et al.* 1996; Dunlop & Özdemir 1997). Sahota *et al.* (1995) reported low S-ratios at palaeo-oxidation fronts in Atlantic sediment cores and interpreted them as resulting from a higher content of imperfect antiferromagnetic components (i.e. goethite and haematite). If haematite or goethite were responsible for the high-coercivity signal in the hysteresis loops, these minerals would have to be at least 100 times as abundant as the relatively low-coercivity magnetite, because of the low magnetizations of haematite and goethite. Such abundant haematite or goethite would be evident in the thermomagnetic curves, which only indicate the presence of magnetite (Fig. 3), with no haematite or goethite. Moreover, the enrichment of Fe oxides (Fig. 1) at this level relative to other levels in the oxidized sapropel is not sufficient to accommodate such large amounts of goethite or haematite. We propose that the wasp-waisted shape of the hysteresis loops at the FeRB is caused by a mixture of high-coercivity SD grains and large SP grains, as modelled by Tauxe *et al.* (1996). The SP grains could be chemical precipitates of Fe oxides and the high-coercivity grains could be magnetosomes of magnetotactic bacteria. Amorphous Fe oxide probably formed as well. Tarduno & Wilkison (1996) and Tarduno *et al.* (1998) found that the coercivity peak at the FeRB in Pacific Ocean sediments was produced by an unusually abundant population of distinctively sized and

elongated high-coercivity bacterial SD magnetite (35–120 nm) at the FeRB.

The diagenetic Fe oxides higher in the oxidized sapropel are older than those between the MnRB and FeRB, because of the downward-moving direction of the oxidation front. The aged Fe oxides have lower coercivity than those at the FeRB, but they retain relatively high coercivity. Also, the S-ratio is not as low in these sediments (Fig. 4). The hysteresis loops are not wasp-waisted, but pot-bellied hysteresis loops occur in this zone. Such loops indicate SD grains, possibly mixed with small SP grains (Roberts *et al.* 1995; Tauxe *et al.* 1996). We suggest that the freshly formed magnetosomes, SP grains and amorphous Fe oxide that initially precipitated at the FeRB have aged into grains that have a lower but still a relatively high coercivity (possibly caused by fossil magnetosomes or partially maghemitized magnetite). The resulting magnetic mixture is an efficient ARM carrier.

Around the FeRB, there is a zone in the top of the sapropel with relatively low $ARM_{300\ mT}$ (Fig. 2) and consequently χ_{ARM}/χ_{in} and ARM/M_{rs} values (Fig. 5). Possibly, the Fe monosulphide phase that is inferred to cause high values χ_{ARM}/χ_{in} and ARM/M_{rs} within the sapropel has been oxidized away and has not yet been replaced by the ARM-carrying Fe oxide phase that is present in the oxidized sapropel.

There are indications that the high-coercivity SD grains that form at the FeRB survive burial beneath the FeRB. Magnetic expressions of palaeo-oxidation fronts (buried beneath the present FeRB) have been reported in the Pacific (Tarduno & Wilkison 1996; Tarduno *et al.* 1998) and the Atlantic (Sahota *et al.* 1995) oceans. Roberts *et al.* (1999) reported a somewhat lower S-ratio in the top of a Pliocene sapropel (*c.* 1.5 Ma) that is buried 50 m below the Mediterranean seafloor. This suggests that this particular sapropel was partially oxidized by an oxidation front before it was buried and that the magnetic expression of this palaeo-oxidation front survived burial. In addition, high ARM intensities were found above sapropels of up to 1 Myr in age at depths of up to 35 m in an eastern Mediterranean piston core (Langereis *et al.* 1997; van Santvoort *et al.* 1997). These findings suggest that the magnetic expressions of palaeo-oxidation fronts survive in the Mediterranean as well.

Coercivity features and Fe-oxide enrichment in the oxidized sapropel are more extreme in BC19 than in ABC26 (Fig. 4). This is caused by the differences in C_{org} and Fe_{pyr} contents of S1 at the two sites (Fig. 1). In BC19 these contents are higher than in ABC26. Consequently, the downward movement of the oxidation front has been slowed more by oxidation of organic matter and pyrite in BC19 than in ABC26. The peak-like enrichment of Fe oxides at the top of the sapropel may suggest a standstill of the oxidation front at the site of BC19. A downward-moving front may result in a more gradually increasing Fe oxide enrichment, as observed in ABC26 (Fig. 1).

5 CONCLUSIONS

From combined geochemical and magnetic analyses we can determine the history of deposition, dissolution and formation of sedimentary magnetic Fe compounds around the most recent eastern Mediterranean sapropel. The non-steady-state diagenetic systems in the past and present and the resulting Fe mineralogy of the sediments are summarized in Fig. 7.

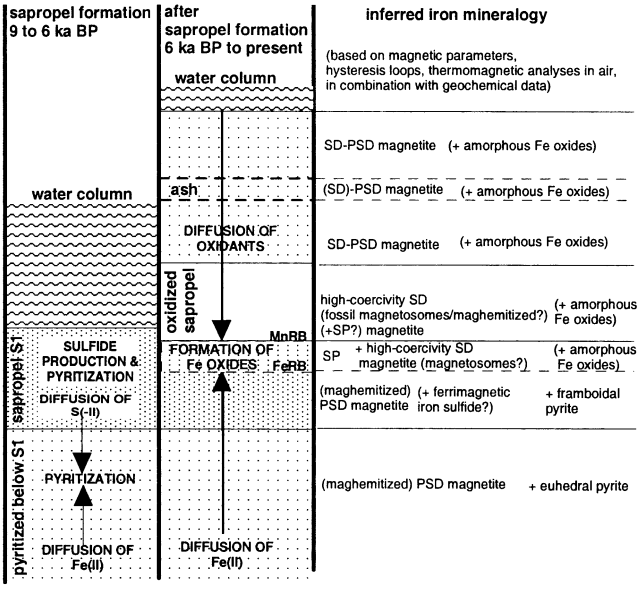

Figure 7. Schematic representation of the diagenetic systems during and after formation of sapropel S1 and inferred Fe mineralogy in the eastern Mediterranean.

5.1 Detrital sedimentation and sapropel diagenesis

Mediterranean sediments receive variable amounts of SD to PSD magnetite grains from dust. Furthermore, PSD magnetite is enriched in the Santorini ash layer. During deposition of the sapropel, the Fe bearing minerals are affected by reductive dissolution of Fe oxides and subsequent pyrite formation. This process affects both the sapropel and the pyritized zone below S1. After sapropel deposition, reductive dissolution of Fe oxides continues in the sapropel and below. However, large-scale pyrite formation does not take place anymore, because the sapropel and pyritized zone below S1 are no longer anoxic/sulphidic, but suboxic. Two different types of pyrite, presumably mainly framboidal pyrite in the sapropel and euhedral pyrite in the pyritized zone below S1, can be identified in thermomagnetic analyses. Reductive dissolution and pyritization result in lower magnetic intensities, a coarser grain size, and maghemitization, causing slightly higher magnetic coercivities. These magnetic dissolution features are clear in the pyritized zone below S1, whereas the sapropel itself seems to contain another magnetic phase, perhaps a ferrimagnetic Fe monosulphide. This Fe monosulphide probably formed during later stages of diagenesis and could therefore cause a palaeomagnetic overprint in these sapropel sediments.

5.2 Post-sapropel oxic diagenesis

After sapropel deposition, eastern Mediterranean bottom waters were reoxygenated and a progressively downward-moving oxidation front has oxidized the upper part of the sapropel. This oxidation has produced Fe oxides with relatively high coercivity. Several downcore changes in magnetic properties suggest that there is a sequence of processes and products leading to the formation of Fe oxides at the oxidation front. The site of active oxidation, where dissolved Fe^{2+} is transformed into Fe oxides, is situated between the MnRB and FeRB. It divides the oxic sediments above from the suboxic

sapropel and pyritized zone below S1. The oxidation results in the formation of high-coercivity grains (presumably magnetosomes) as well as SP grains (indicated by wasp-waisted hysteresis loops) and amorphous Fe oxide at the FeRB. Subsequently, these fresh Fe oxides age to grains with on average a higher $ARM_{300\ mT\ and}$ a slightly lower coercivity (possibly fossil magnetosomes or partially maghemitized magnetite).

Fe_{pyr} and C_{org} contents are important determinants of the amount of diagenetic Fe oxides formed and their subsequent magnetic expression. Higher pyrite contents provide more Fe for Fe oxide formation. Furthermore, higher initial amounts of reduced materials (organic matter and pyrite) lower the rate of movement of the oxidation front, which in turn intensifies the diagenetic Fe oxide formation and its magnetic expression. There are indications that the high-coercivity SD grains that formed at palaeo-oxidation fronts survive burial at depth.

ACKNOWLEDGMENTS

We thank the crew and scientific parties of the Tyro (1987) and Marion Dufresne (1991) expeditions, and H. J. Meijer, P. J. Verplak, H. C. de Waard, G. N. Nobbe, D. van de Meent, C. Slomp and A. Rutten for their help with obtaining and analysing the samples. The journal reviewers A. Roberts and H. Stanjek are thanked for their constructive comments. Supported by NWO/ALW, EU-MAST Programs CT93-0051 and CT97-0137 and a visiting fellowship (HFP) to the Institute for Rock Magnetism (Minneapolis, USA) with funding from the US NSF. Conducted under the programme of the Vening Meinesz Research School of Geodynamics and the Netherlands Research School of Sedimentary Geology (publication # 20001002).

REFERENCES

Banerjee, S.K., King, J. & Marvin, J., 1981. A rapid method for magnetic granulometry with applications to environmental studies, *Geophys. Res. Lett.,* **8,** 333–336.

Bazylinski, D.A., 1996. Controlled biomineralization of magnetic minerals by magnetotactic bacteria, *Chem. Geol.,* **132,** 191–198.

Bierens de Haan, S., 1991. A review of the rate of pyrite oxidation in aqueous systems at low temperature, *Earth Sci. Rev.,* **31,** 1–10.

Bloemendal, J., King, J.W., Hall, F.R. & Doh, S.-J., 1992. Rock magnetism of Late Neogene and Pleistocene deep-sea sediments: relationship to sediment source, diagenetic processes, and sediment lithology, *J. geophys. Res.,* **97,** 4361–4375.

Bloemendal, J., King, J.W., Hunt, A., Demenocal, P.B. & Hayashida, A., 1993. Origin of the sedimentary magnetic record at Ocean Drilling Program Sites on the Owen Ridge, Western Arabian Sea, *J. geophys. Res.,* **98,** 4199–4219.

Brothers, L.A., Engel, M.H. & Elmore, R.D., 1996. The late diagenetic conversion of pyrite to magnetite by organically complexed ferric iron, *Chem. Geol.,* **130,** 1–14.

Burdige, D.J., 1993. The biogeochemistry of manganese and iron reduction in marine sediments, *Earth Sci. Rev.,* **35,** 249–284.

Calvert, S.E., Nielsen, B. & Fontugne, M.R., 1992. Evidence from nitrogen isotope ratios for enhanced productivity during formation of eastern Mediterranean sapropels, *Nature,* **359,** 223–225.

Canfield, D.E. & Berner, R.A., 1987. Dissolution and pyritization of magnetite in anoxic marine sediments, *Geochim. Cosmochim. Acta,* **51,** 645–659.

Channell, J.E.T., Hawthorne, T. & Torii, M., 1990. Contrasting magnetic properties in Leg 107 sediments: preservation and alteration of titanomagnetite at adjacent sites, in *Proc. ODP, Sci. Res.,* Vol. 107, pp. 113–128, eds Kastens, K.A. *et al*., ODP, College Station, TX.

Cornell, R.M. & Schwertmann, U., 1996. *The Iron Oxides—Structure, Properties, Reactions, Occurrence and Uses,* VCH Verlagsgesellschaft mbH, Weinheim.

Dekkers, M.J., Langereis, C.G., Vriend, S.P., van Santvoort, P.J.M. & Lange, G.J., 1994. Fuzzy c-means cluster analysis of early diagenetic effects on natural remanent magnetisation acquisition in a 1.1 Myr piston core from the Central Mediterranean, *Physics Earth Planet. Int.,* **85,** 155–171.

de Pruysers, P.A., Lange, G.J., Middelburg, J.J. & Hydes, D.J., 1993. The diagenetic formation of metal-rich layers in sapropel-containing sediments in the eastern Mediterranean, *Geochim. Cosmochim. Acta,* **57,** 527–536.

Dunlop, D.J. & Özdemir, Ö., 1997. *Rock Magnetism—Fundamentals and Frontiers,* Cambridge University Press, Cambridge.

Emeis, K.-C. & Party, S.S., 1996. Paleoceanography and sapropel introduction, in *Proc. ODP., Init. Repts,* Vol. 160, pp. 21–28, eds Emeis, K.-C. *et al*., ODP, College Station, TX.

Frankel, R.B. & Bazylinski, D.A., 1994. Magnetotaxis and magnetic particles in bacteria, *Hyperfine Interacts,* **90,** 135–142.

Frederichs, T., Bleil, U., Däumler, K., von Dobeneck, T. & Schmidt, A., 1999. The magnetic view on the marine paleo-environment: parameters, techniques and potentials of rock magnetic studies as a key to paleoclimatic and paleoceanographic changes, in *Use of Proxies in Paleoceanography: Examples from the South Atlantic,* pp. 575–599, eds Fischer, G. & Wefer, G., Springer-Verlag, Berlin.

Heider, F., Dunlop, D.J. & Soffel, H.C., 1992. Low-temperature and alternating field demagnetization of saturation remanence and thermoremanence in magnetite grains (0.037 μm to 5 mm), *J. geophys. Res.,* **97,** 9371–9381.

Karlin, R., 1990a. Magnetic diagenesis in marine sediments from the Oregon continental margin, *J. geophys. Res.,* **95,** 4405–4419.

Karlin, R., 1990b. Magnetic mineral diagenesis in suboxic sediments at Bettis Site W-N, NE Pacific Ocean, *J. geophys. Res.,* **95,** 4421–4436.

Karlin, R. & Levi, S., 1985. Geochemical and sedimentological control of the magnetic properties of hemipelagic sediments, *J. geophys. Res.,* **90,** 10 373–10 392.

King, J., Banerjee, S.K., Marvin, J. & Özdemir, Ö., 1982. A comparison of different magnetic methods for determining the relative grain size of magnetite in natural materials: some results from lake sediments, *Earth planet. Sci. Lett,* **59,** 404–419.

Langereis, C.G., de Dekkers, M.J., Lange, G.J., Paterne, M. & van Santvoort, P.J.M., 1997. Magnetostratigraphy and astronomical calibration of the last 1.1 Myr from an eastern Mediterranean piston core and dating of short events in the Brunhes, *Geophys. J. Int.,* **129,** 75–94.

Leslie, B.W., Hammond, D.E., Berelson, W.M. & Lund, S.P., 1990a. Diagenesis in anoxic sediments from the California continental borderland and its influence on iron, sulfur, and magnetite behavior, *J. geophys. Res.,* **95,** 4453–4470.

Leslie, B.W., Lund, S.P. & Hammond, D.E., 1990b. Rock magnetic evidence for the dissolution and authigenic growth of magnetic minerals within anoxic marine sediments of the California continental borderland, *J. geophys. Res.,* **95,** 4437–4452.

Lourens, L.J., Antonarakou, A., Hilgen, F.J., van Hoof, A.A.M., Vergnaud-Grazzini, C. & Zachariasse, W.J., 1996. Evaluation of the Plio-Pleistocene astronomical time scale, *Paleoceanography,* **11,** 391–413.

Maher, B.A., 1988. Magnetic properties of some synthetic sub-micron magnetites, *Geophys. J.,* **94,** 83–96.

Mullender, T.A.T., van Velzen, A.J. & Dekkers, M.J., 1993. Continuous drift correction and separate identification of ferrimagnetic and paramagnetic contributions in thermomagnetic runs, *Geophys J. Int.,* **114,** 663–672.

Passier, H.F., Middelburg, J.J., van Os, B.J.H. & Lange, G.J., 1996. Diagenetic pyritisation under eastern Mediterranean sapropels caused by downward sulphide diffusion, *Geochim. Cosmochim. Acta,* **60,** 751–763.

Passier, H.F., de Middelburg, J.J., Lange, G.J. & Böttcher, M.E., 1997. Pyrite contents, microtextures, and sulfur isotopes in relation to formation of the youngest eastern Mediterranean sapropel, *Geology,* **25,** 519–522.

Passier, H.F., de Dekkers, M.J. & Lange, G.J., 1998. Sediment chemistry and magnetic properties in an anomalously reducing core from the eastern Mediterranean Sea, *Chem. Geol.,* **152,** 287–306.

Passier, H.F., de Middelburg, J., Lange, G.J. & Böttcher, M.E., 1999. Modes of sapropel formation in the eastern Mediterranean: some constraints based on pyrite properties, *Mar. Geol.,* **153,** 199–219.

Richter, C., Roberts, A.P., Stoner, J.S., Benning, L.D. & Chi, C.T., 1998. Magnetostratigraphy of Pliocene-Pleistocene sediments from the eastern Mediterranean Sea, in *Proc. ODP, Sci. Results,* Vol. 160, pp. 61–73, eds. Robertson, A.H.F., Emeis, K.-C., Richter, C. & Camerlenghi, A., ODP, College Station, TX.

Roberts, A.P., Cui, Y. & Verosub, K.L., 1995. Wasp-waisted hysteresis loops: mineral magnetic characteristics and discrimination of components in mixed magnetic systems, *J. geophys. Res.,* **100,** 17 909–17 924.

Roberts, A.P., Stoner, J.S. & Richter, C., 1999. Diagenetic magnetic enhancement of sapropels from the eastern Mediterranean Sea, *Mar. Geol.,* **153,** 103–116.

Robinson, S., 1990. Applications for whole-core magnetic susceptibility measurements of deep-sea sediments: Leg 115 results, in *Proc ODP, Sci Results,* Vol, 115, pp. 737–770, ed. Duncan, R.A., Ocean Drilling Program, College Station, TX.

Rohling, E.J., 1994. Review and new aspects concerning the formation of eastern Mediterranean sapropels, *Mar. Geol.,* **122,** 1–28.

Rossignol-Strick, M., 1999. The Holocene climatic optimum and pollen records of sapropel 1 in the eastern Mediterranean, *Quat. Sci. Rev.,* **18,** 515–530.

Rossignol-Strick, M., Nesteroff, W., Olive, P. & Vergnaud-Grazzini, C., 1982. After the deluge: Mediterranean stagnation and sapropel formation, *Nature,* **295,** 105–110.

Sahota, J.T.S., Robinson, S.G. & Oldfield, F., 1995. Magnetic measurements used to identify paleoxidation fronts in deep-sea sediments from the Madeira Abyssal Plain, *Geophys. Res. Lett.,* **22,** 1961–1964.

Schwartz, M., Lund, S.P., Hammond, D.E., Schwartz, R. & Wong, K., 1997. Early sediment diagenesis on the Blake/Bahama Outer Ridge, North Atlantic Ocean, and its effects on sediment magnetism, *J. geophys. Res.,* **102,** 7903–7914.

Tarduno, J.A. & Wilkison, S.L., 1996. Non-steady state magnetic mineral reduction, chemical lock-in, and delayed remanence acquisition in pelagic sediments, *Earth planet. Sci. Lett,* **144,** 315–326.

Tarduno, J.A., Tian, W. & Wilkison, S., 1998. Biogeochemical remanent magnetization in pelagic sediments of the western equatorial Pacific Ocean, *Geophys. Res. Lett,* **25,** 3987–3990.

Tauxe, L., Mullender, T.A.T. & Pick, T., 1996. Potbellies, wasp-waists, and superparamagnetism in magnetic hysteresis, *J. geophys. Res.,* **101,** 571–583.

Thompson, R. & Oldfield, F., 1986. *Environmental Magnetism,* Allen & Unwin, London.

van Santvoort, P.J.M., Lange, G.J., Thomson, J., Cussen, H., Wilson, T.R.S., Krom, M.D. & Ströhle, K.D., 1996. Active post-depositional oxidation of the most recent sapropel (S1) in sediments of the eastern Mediterranean Sea, *Geochim. Cosmochim. Acta,* **60,** 4007–4024.

van Santvoort, P.J.M., Lange, G.J., Langereis, C.G. & Dekkers, M.J., 1997. Geochemical and paleomagnetic evidence for the occurrence of 'missing' sapropels in eastern Mediterranean sediments, *Paleoceanography,* **12,** 773–786.

Wehausen, R. & Brumsack, H.-J., 1999. Cyclic variations in the chemical composition of eastern Mediterranean Pliocene sediments: a key for understanding sapropel formation, *Mar. Geol.,* **153,** 161–176.